

## Accepted Manuscript

Investigation and Simulation of the Transport of Gas Containing Mercury in Microporous Silica Membranes

Guozhao Ji, Anthe George, Vicky Skoulou, Graham Reed, Marcos Millan, Kamel Hooman, Suresh K. Bhatia, João C. Diniz da Costa

PII: S0009-2509(18)30368-3  
DOI: <https://doi.org/10.1016/j.ces.2018.06.006>  
Reference: CES 14280

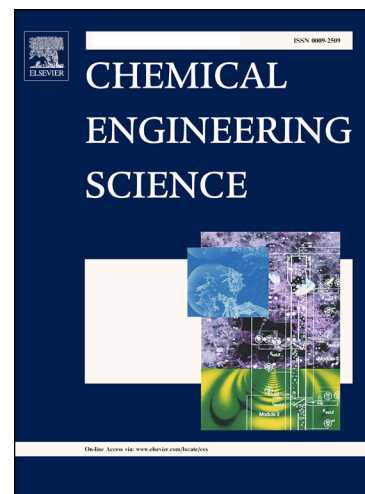
To appear in: *Chemical Engineering Science*

Received Date: 27 February 2018  
Revised Date: 9 May 2018  
Accepted Date: 1 June 2018

Please cite this article as: G. Ji, A. George, V. Skoulou, G. Reed, M. Millan, K. Hooman, S.K. Bhatia, J.C. Diniz da Costa, Investigation and Simulation of the Transport of Gas Containing Mercury in Microporous Silica Membranes, *Chemical Engineering Science* (2018), doi: <https://doi.org/10.1016/j.ces.2018.06.006>

This is a PDF file of an unedited manuscript that has been accepted for publication. As a service to our customers we are providing this early version of the manuscript. The manuscript will undergo copyediting, typesetting, and review of the resulting proof before it is published in its final form. Please note that during the production process errors may be discovered which could affect the content, and all legal disclaimers that apply to the journal pertain.

© 2018. This manuscript version is made available under the CC-BY-NC-ND 4.0 license <http://creativecommons.org/licenses/by-nc-nd/4.0/>



## Investigation and Simulation of the Transport of Gas Containing Mercury in Microporous Silica Membranes

Guozhao Ji<sup>a,b</sup>, Anthe George<sup>c,d</sup>, Vicky Skoulou<sup>c,e</sup>, Graham Reed<sup>c</sup>, Marcos Millan<sup>c</sup>, Kamel Hooman<sup>f</sup>, Suresh K. Bhatia<sup>a</sup>, João C. Diniz da Costa<sup>a\*</sup>

<sup>a</sup>The University of Queensland, FIM<sup>2</sup>Lab – Functional Interfacial Materials and Membranes Laboratory, School of Chemical Engineering, Brisbane, Qld 4072, Australia.

<sup>b</sup>School of Environmental Science & Technology, Dalian University of Technology, Dalian 116024, Liaoning, China.

<sup>c</sup>Department of Chemical Engineering, Imperial College London, South Kensington Campus, London SW7 2AZ, United Kingdom.

<sup>d</sup>Sandia National Laboratories, 7011 East Avenue, Livermore CA, 94550, United States of America.

<sup>e</sup>Chemical Engineering, School of Engineering and Computer Science, University of Hull, Cottingham Rd, Hull HU6 7RX, United Kingdom.

<sup>f</sup>The University of Queensland, School of Mining and Mechanical Engineering, Brisbane, Qld 4072, Australia.

### Abstract

This work investigates the effect of condensable Hg vapour on the transport of N<sub>2</sub> gas across cobalt oxide silica (CoOxSi) membranes. Experimental results suggest that Hg significantly affects N<sub>2</sub> permeation at 100 and 200°C, though this effect is negligible at 300°C. This effect was found to have a correlation with Hg adsorption on CoOxSi xerogels. In order to understand the Hg effect in the transport phenomena of N<sub>2</sub> permeation, the oscillator model was used to model gas transport through pores with different sizes. By including effective medium theory (EMT), the oscillator model fitted well the experimental results and gave good prediction of mass transfer in ultra-microporous materials with a tri-modal pore size distribution, such as silica membranes. It is postulated that Hg seeks lower level potentials in micro-pores, and therefore Hg molecules tend to block small pores (2.5-4Å from 2.9Å), or reduce the average pore size of larger pores (6.7-7.8Å and 12-14Å). Although N<sub>2</sub> permeation decreased with the presence of Hg, it did not decrease when the Hg load was increased by a factor of ten; this strongly suggests the adsorption of Hg molecules in the smaller pores (2.5-4.0Å), or along the pore wall for the larger pore ranges (6.7-7.8Å and 12-14Å).

Keywords: silica membrane; mercury adsorption; micropore transport; effective media theory; oscillator model.

## 1. Introduction

Porous inorganic membranes have evolved since the early 1990s, when gas separation values were below 10, to values close or even higher than 1000. This major achievement has been possible by the control of the pore sizes of the membranes, allowing for the smaller gas molecule to permeate, whilst blocking the passage of the larger gas molecule. This is known as a molecular sieving mechanism as a result of molecular exclusion. Early major improvements in separation performance were reported by Verweij's group by late 1990s [1], where silica thin-films were prepared on the top of high quality interlayer substrates in clean rooms. This approach greatly reduced defects, and silica membranes reached  $H_2/CO_2$  selectivities of around 100. The separation performance of membranes varies from case to case, based on the porous structure, adsorption properties and thickness of selective layers. In addition, mass transfer across a membrane is dependent on many factors such as membrane structure, gas property, temperature, pressure, and gas concentration which all affect gas fluxes (or production) and gas separation (or quality/purity). Therefore, different operating conditions require precise models to predict and explain the membrane performance.

In the case of silica derived membranes complying with molecular sieving transport, gas molecules in the gas phase must adsorb on the surface or at the pore entrance of the membrane. Due to a difference in concentration from the high pressure side (i.e., feed domain) to the low pressure side (i.e., permeate domain), this results in a concentration gradient which allows the gas molecules to jump between adsorption sites within the pores of the membrane [2-4]. This mechanism is known as surface diffusion. When pore size is reduced to dimensions below the Lennard Jones (L-J) diameter of the gas molecules (also known as the kinetic diameter), molecular attraction by physical adsorption is no longer feasible. In this case, there is a repulsive force between the pore entrance and the molecule which stops the molecule from entering. In other words, the potential for a molecule entering the pore is too high. Hence, the gas molecule requires much more energy to be able to diffuse through these pores smaller than the molecular L-J diameter [5, 6]. In this process, the gas kinetic energy is converted to potential energy when a gas molecule approaches a pore. In order to increase the gas potential and likewise permeation, energy must be supplied in terms of thermal energy which increases the kinetic energy. Since the gas needs extra energy to activate the transport, this process shows temperature dependency and is called activated transport which is generally a characteristic of molecular sieving silica membranes. This unique transport is usually

observed in ultra-microporous membranes with pore sizes below 5 Å, as it is the case for silica derived membrane for separating H<sub>2</sub> or He from other larger gases [7-9].

Surface diffusion and activated transport are the most common mechanisms in ultra-microporous membrane separation. Krishna et al. [10] studied the effect of high binary gas selectivity caused by strong adsorption from one component and used Molecular Dynamics (MD) to simulate transport properties, as adsorption also affects gas selectivities. For activated transport, the gas permeation in ultra-microporous membranes generally decreases as a function of the gas kinetic diameter, so the membrane separates gases based on molecular size [11-14]. The separation of industrial gas is more challenging due to complex mixtures of gases, water vapour and condensable vapours. Recently, Deonarine et al. [15] reported that He permeance decreased by ~17% in a cobalt oxide silica membrane when exposed to a model tar compound (0.24 mol% toluene). This demonstrates the effect of condensable vapours in micro-pore structures. Yoshioka et al. [16] used a molecular dynamics simulation to report the effect of condensable gas filling in microporous silica membranes. These limited studies clearly show that the effect of condensable gases can be significant in the separation of industrial gases.

A potential application of silica membranes is the separation of H<sub>2</sub> from syngas mixtures such as in coal gasification processes [17, 18]. A common feature of coal derived syngas mixture is the presence of mercury at small concentrations [19, 20]. There is a large body of research and engineering works published in the area of mercury capture in coal power stations to meet regulatory emissions standards, using generally high temperature ceramic filters or carbon as adsorbents. However, there is no literature on the transport of mercury in ultra-microporous materials. Mercury in its vapour form is a condensable gas and it is postulated that mercury could significantly affect the transport of gases in microporous membranes. To test this postulation, the performance of cobalt oxide silica membranes were investigated for gas streams spiked with mercury at various temperatures, feed flow rates and mercury concentration. This work was accompanied by mercury adsorption studies on cobalt oxide silica xerogels. To predict the permeation of gases in the presence of mercury, the oscillator model was used to determine the diffusion coefficient and adsorption equilibrium constant. Further, the effective medium theory (EMT) model was considered by bearing in mind the pore size distribution in silica derived materials. These models were validated the experimental results and explained the effect of mercury adsorption/condensation on the transport of gases in ultra-microporous materials.

## 2. Experiment

Cobalt oxide silica (CoO<sub>x</sub>Si) membranes were prepared on  $\gamma$ -alumina coated  $\alpha$ -alumina tubes (110 mm length; 10 mm diameter) supplied by Noritake Co. Ltd., Japan. The CoO<sub>x</sub>Si sol-gel solutions were prepared from tetraethyl orthosilane (TEOS), ethanol (EtOH), 30% hydrogen peroxide (H<sub>2</sub>O<sub>2</sub>) in water (H<sub>2</sub>O) and cobalt nitrate hexhydrate (Co(NO<sub>3</sub>)<sub>2</sub>·6H<sub>2</sub>O) with the molar ratio of 255 EtOH : 4 TEOS : 1 Co(NO<sub>3</sub>)<sub>2</sub>·6H<sub>2</sub>O : 9 H<sub>2</sub>O<sub>2</sub> : 40 H<sub>2</sub>O. The dip-coating used a controlled immersion time of 1 min, and immersion/withdrawal speed of 2 cm min<sup>-1</sup>. Subsequently, each layer was calcined at 630 °C in ambient air with a dwell time of 4 h and a heating and cooling rate of 1 °C min<sup>-1</sup>. A total of 2 CoO<sub>x</sub>Si layers were coated onto the outer surface of the alumina tube.

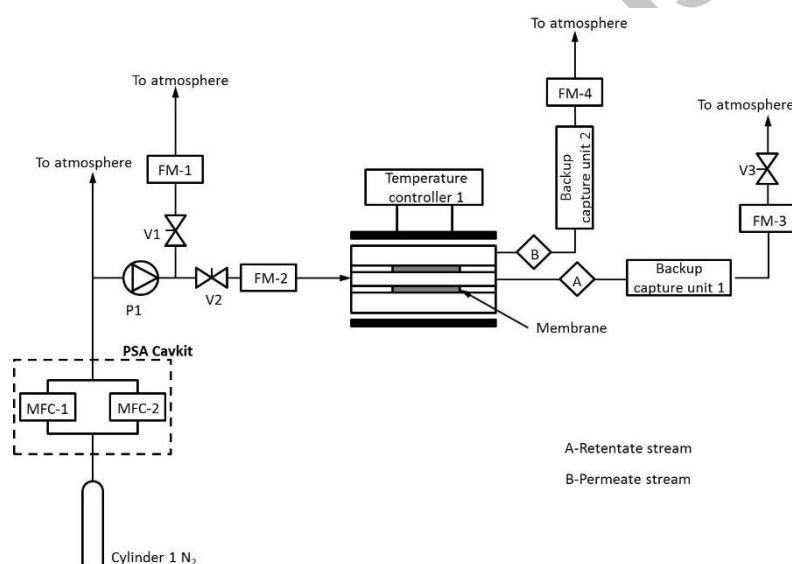


Fig. 1 Schematic diagram of the experimental setup

Fig. 1 depicts the apparatus used to conduct the Hg adsorption and gas permeation experimental work. In order to comply with Occupational Health and Safety regulations, H<sub>2</sub> was replaced with inert N<sub>2</sub> gas. The membranes were subjected sequentially to pure N<sub>2</sub> and then N<sub>2</sub> gas streams spiked with 30 to 300 ngHg L<sup>-1</sup>, at temperatures from 100 to 300 °C. For each experimental temperature set point, the temperature was held for 1 h prior to experimental work. PSA Cavkit equipment was used as the Hg controlled emission unit. A heat source in the PSA Cavkit allowed for Hg to vaporise and the concentration of Hg was adjusted by two mass flow controllers (MFC-1 and MFC-2). The excess gas was vented. The gas mass balance was checked by a series of flow meters in the feed (FM-2), retentate (FM-3) and permeate (FM-4) streams. The Hg mass balance was performed by capturing Hg in the permeate and retentate streams using an activated carbon sorbent (Norit

Darco Hg) as the back-up capture. The two back-up capture units were analysed using a LECO AMA 254, a dedicated spectrophotometric instrument for measuring Hg.

In the case of Hg adsorption, the experimental rig was the same as in Fig. 1, the only difference is that the membrane unit was replaced by a tube containing a small glass wool holder to hold an amount of CoOxSi xerogel as sorbent. In this case, there was just one outlet stream “B” in Fig. 1. The xerogels were exposed to N<sub>2</sub> gas streams spiked with 30 to 300 ngHg L<sup>-1</sup> at temperatures from 100 to 300°C. After a single exposure test, the CoOxSi sample was analysed by a LECO AMA 254 spectrophotometric instrument for measuring Hg. The CoOxSi xerogels were prepared and calcined in the same manner as the CoOxSi membranes.

### 3. Transport modelling

#### 3.1 Gas transport modelling across the silica membrane

Gas transport in nano-pores behaves very differently from that in the bulk fluid. Whilst the latter is dominated by gas-gas interactions, in nano-pores the mean free path of gas molecules is comparable to the pore size, so that their motion is strongly affected by wall-fluid van der Waals interactions. To capture the influence of this interaction on the transport we used the Oscillator model of Bhatia and co-workers [30], considering the motion of single site L-J molecules in a cylindrical capillary, with diffuse reflection at the pore walls. This model solves the equations of motion of the molecules under the influence of the fluid-wall interaction potential field  $\phi(r)$ , while considering a Boltzmann distribution of energies, and yields the diffusion coefficient  $D$  as

$$D = \frac{2}{\pi m \int_0^\infty r e^{-\frac{\phi(r)}{k_B T}} dr} \int_0^\infty e^{-\frac{\phi(r)}{k_B T}} dr \int_0^\infty e^{-\frac{p_r^2}{2mk_B T}} dp_r \int_0^\infty e^{-\frac{p_\theta^2}{2mr^2 k_B T}} dp_\theta \int_{r_{co}(r, p_r, p_\theta)}^{r_{ci}(r, p_r, p_\theta)} \frac{dr'}{p_r(r', r, p_r, p_\theta)} \quad (1)$$

where  $k_B$  is Boltzmann constant,  $T$  is temperature, and  $m$  is molecular mass. Here, the function  $p_r(r', r, p_r, p_\theta)$  is the radial momentum of a particle at radial position  $r'$ , given that it has radial and angular momenta  $p_r$  and  $p_\theta$  at radial position  $r$ , respectively, and is given by

$$p_r(r', r, p_r, p_\theta) = \left\{ 2m[\phi(r) - \phi(r')] + p_r^2(r) + \frac{p_\theta^2}{r^2} \left( 1 - \frac{r'^2}{r^2} \right) \right\}^{1/2} \quad (2)$$

Further,  $r_{cl}(r, p_r, p_\theta)$  and  $r_{co}(r, p_r, p_\theta)$  are the bounds of the oscillation, following  $p_r(r', r, p_r, p_\theta) = 0$ .

The permeate flux through a single pore is generally expressed as [21]:

$$J = \frac{qD}{RT} (-\nabla\mu) \quad (3)$$

where  $q$  is the concentration of gas molecule in the pore, and  $\nabla\mu$  is the chemical potential gradient. For an ideal gas and linear pressure gradient Eq. (3) yields for the permeate flow rate  $F$  as:

$$F = \frac{\pi r_p^2 KD}{RTl} (-\Delta p) \quad (4)$$

where  $K$  is the adsorption equilibrium constant  $q/c$ , in the cylindrical pore. Here  $c$  is the gas phase concentration. For a cylindrical pore with radius  $r_p$  we have:

$$K(r_p) = \frac{2}{r_p^2} \int_0^{r_p} \exp\left(\frac{-\phi(r)}{k_B T}\right) r dr \quad (5)$$

Since the sorbent is amorphous and comprises a range of pore sizes, it is necessary to suitably average the permeance in Eq. (4), and to this end we use effective medium theory. In this theory we define the pore size-dependent conductance  $\lambda$  of a pore with radius  $r_p$  as:

$$\lambda(r_p) = \frac{\pi r_p^2 KD}{RTl} \quad (6)$$

and replace the pore network with an effective one having pores of uniform conductance. The pore size distribution (PSD) of ultra-microporous silica membranes range between 2.5-4Å, with a proportion of pores smaller than 3Å [22]. However, it has been demonstrated by using Positron Annihilation Spectroscopy (PALS) that amorphous silica matrices have narrow tri-modal pore size distribution at 2.5-4Å, 6.7-7.8Å and 12-14Å [23]. Silica derived membranes generally have 4-6 silica layers, and commonly have He and H<sub>2</sub> permeation rates that are two to three orders of magnitude higher than that of N<sub>2</sub> which has a kinetic diameter of 3.6 Å. This suggests that the permeation of gases is controlled by constrictions with pore sizes below 3.6 Å, as N<sub>2</sub> rarely accesses these smaller pores due to their high entry barrier. Hence, the conventional nitrogen adsorption method generally used to determine PSD is not conducive to determining the PSD for pores below 3.6 Å in size. To overcome this drawback, we used the results of Yoshika et al. [24, 25], who employed molecular dynamics simulation to calculate the PSD of silica, which provides a good approximation of the CoOxSi materials used in this work. Fig. 2 shows the PSD in terms of volume density and number density, which are related by Eq. (7) as shown below:

$$f_N(r_p) = \frac{f_v(r_p)}{r_p^2 \int_0^\infty \frac{f_v(r_p)}{r_p^2} dr_p} \quad (7)$$

where  $f_v$  is the PSD volume density and  $f_N$  is the PSD number density. Three major peaks are evident around the pore sizes 0.1, 0.18 and 0.26 nm. The pores in silica are formed by rings with different number of atoms. These results correspond to 4-membered rings, 5-membered rings and 6-membered rings using ab initio calculations [26].

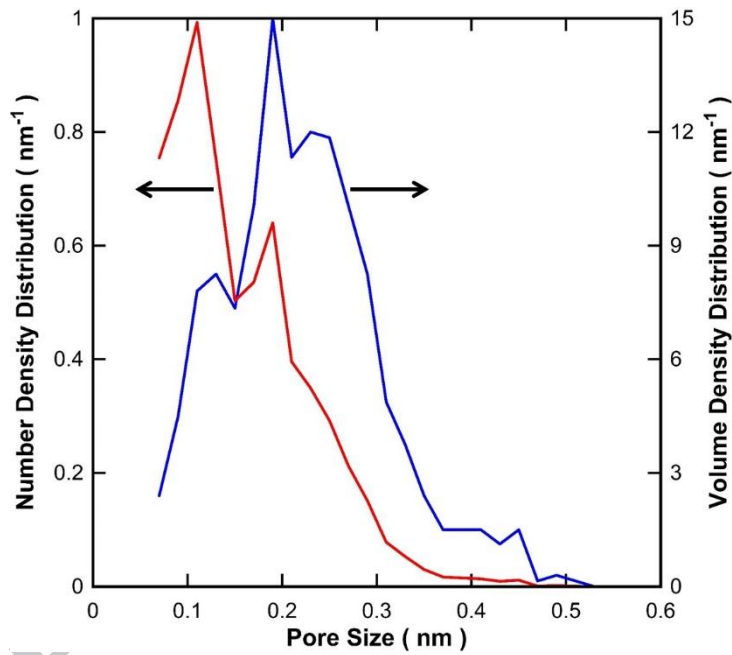


Fig. 2 The PSD in terms of volume density and number density

Eq. (6) shows that the conductance is a function of pore size. The EMT conductance is given by the solution of:

$$\left\langle \frac{\lambda(r_p) - \lambda_e}{\lambda(r_p) + \left(\frac{N}{2} - 1\right)\lambda_e} \right\rangle = 0 \quad (8)$$

where  $\langle \rangle$  represents the average over the pore size number distribution. The permeate flow rate may be expressed as:

$$F = \frac{\varepsilon_p \lambda_e l}{\tau_l L} \Delta p \quad (9)$$

where  $L$  is the membrane thickness,  $\varepsilon_p$  is the porosity and  $\tau_l$  is the tortuosity.

### 3.2 The model of Hg vapour adsorption

Hg vapour possibly adsorbs from a Hg/N<sub>2</sub> mixture on to the pore wall, and could cause pore blockage, depending on how strong the Hg vapour adsorption is. The physical adsorption is likely to occur when the potential energy for Hg in the pore is lower than that in the gas phase. The potential in a cylindrical pore can be obtained from L-J 12-6 potential [27], and is defined as:

$$\phi(r) = 8\varepsilon\eta r_p \int_0^\infty \int_0^{2\pi} \frac{\sigma^{12}}{\left[r_p^2 + r^2 - 2r_p r \cos \theta + z^2\right]^6} - \frac{\sigma^6}{\left[r_p^2 + r^2 - 2r_p r \cos \theta + z^2\right]^3} d\theta dz \quad (10)$$

where  $\eta$  is the real density of sites on the pore surface,  $\sigma$  and  $\varepsilon$  are the L-J constants. For different types of atoms, the constants are estimated by Lorentz Berthelot mixing rules [5, 6, 28]

$$\sigma_{AB} = \frac{1}{2}(\sigma_A + \sigma_B), \quad \varepsilon_{AB} = \sqrt{\varepsilon_A \varepsilon_B} \quad (11)$$

Table 1. lists the L-J parameters of the gases and solid considered in this work [29-31]. It is noteworthy that Hg has a large value of  $\varepsilon/k_B$  which implies that Hg has a higher adsorption equilibrium constant than other gases. The minimum potential of a Hg molecule to pore size in a cylindrical pore is displayed in Fig. 3. It shows that Hg has the strongest interaction with the silica pore sizes  $\sim 0.38$  nm, which means  $\sim 0.38$  nm pores are the most adsorptive to Hg. For pores smaller than 0.3 nm, Hg rarely adsorbs due to the high positive potential of these pores. In the case of N<sub>2</sub> gas, the shallow potential curve (Fig. 3) implies that N<sub>2</sub> has low adsorption capacity.

Table 1. Lennard-Jones parameters used in this model

Parameter	Hg	Si	N <sub>2</sub>
$\sigma$ (nm)	0.289	0.28	0.3572
$\varepsilon/k_B$ (K)	1304	290	93.98

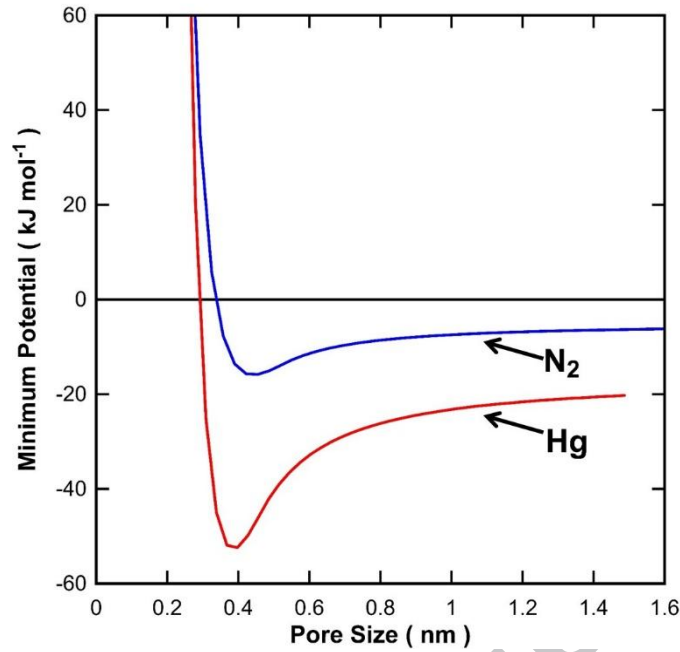


Fig. 3 The minimum potential of Hg and N<sub>2</sub> in different pore sizes (wall atom edge to opposite edge).

The equilibrium constant  $K$  for Hg is expressed by:

$$K = \frac{2}{r_p^2} \int_0^{r_p} \exp\left(\frac{-\phi_{\text{Hg}}(r)}{RT}\right) \cdot r \cdot dr \quad (12)$$

so the Hg concentration in the porous material can be expressed as:

$$q_{\text{Hg}} = \frac{\varepsilon_p K p_{\text{Hg}}}{RT} \quad (13)$$

The number of molecules in a pore is given by:

$$N(r_p) = N_A q_{\text{Hg}} \pi r_p^2 l \quad (14)$$

where  $N_A$  is the Avogadro's constant. If there are more than one Hg molecule in a pore, it is simply assumed that the pore is blocked and not available for gas transportation. If the number of Hg molecules in a pore is less than one, the pore is not completely blocked, but the value  $N(r_p)$  is the same as the probability of pore-blockage. So the probability of a pore still being open is:

$$P(r_p) = 1 - N(r_p) \quad (15)$$

After the membrane is exposed to Hg vapour, some pores are blocked by Hg adsorption. The new pore size distribution in terms of number density is given by:

$$g_N(r) = f_N(r)P(r) \quad (16)$$

Fig. 4 shows the PSD from 0.3 nm where Hg adsorption takes place at different temperatures. For the pores  $< 0.3\text{nm}$ , Hg does not adsorb due to the high potential required for small pores. Therefore, the PSD in the range of  $< 0.3\text{nm}$  is not affected by Hg adsorption. For the pores  $> 0.3\text{nm}$ , the pores are blocked by Hg adsorption and the degree of blockage is temperature dependent. At  $100^\circ\text{C}$ , Hg adsorption is significant and the number of available open pores is greatly reduced and found to be zero from 0.35 to 0.47nm (see Fig. 4). As the temperature increases to 200 and  $300^\circ\text{C}$ , Hg adsorption is less significant and the number of available open pores increases compared to  $100^\circ\text{C}$ . When the adsorption is no longer significant at  $300^\circ\text{C}$ , the PSD is almost the same as the original PSD (without Hg exposure or adsorption).

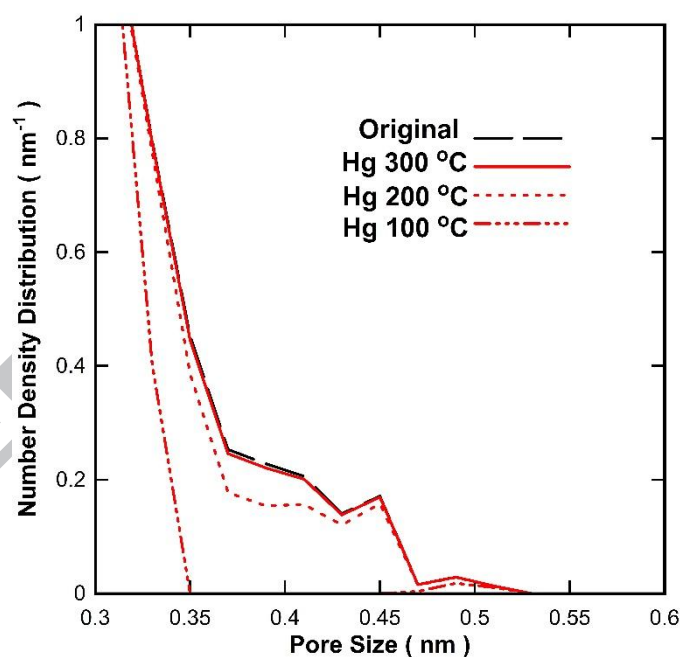


Fig. 4 The effect of Hg adsorption on PSD from 0.3 nm at various temperatures and Hg concentration of  $30\text{ ng L}^{-1}$ .

#### 4 Results and discussion

The permeation of both the uncoated  $\gamma$ -alumina substrate and membrane coated  $\gamma$ -alumina was tested with the simulated  $\text{N}_2$  gas spiked with Hg vapour. The adsorption of the same gas was also measured for alumina and  $\text{CoOxSi}$  powders.

#### 4.1 Adsorption

An initial adsorption experiment was carried out to verify if Hg adsorbed on alumina and CoOxSi powders. The samples were exposed to  $N_2+Hg$   $30 \text{ ng L}^{-1}$  from  $100\text{-}200^\circ\text{C}$  for 60 minutes. Fig. 5 shows that the Hg vapour captured by CoOxSi xerogel is at least 3-fold higher than that of alumina powders. These results strongly suggest that CoOxSi has better affinity to Hg. The trends of adsorption with temperature are consistent with the conventional adsorption theory, as the amount of Hg captured by the samples decreased with the increase in temperature. Particularly important is the significant reduction in Hg vapour capture at  $200^\circ\text{C}$  for the alumina sample, showing values close to zero.

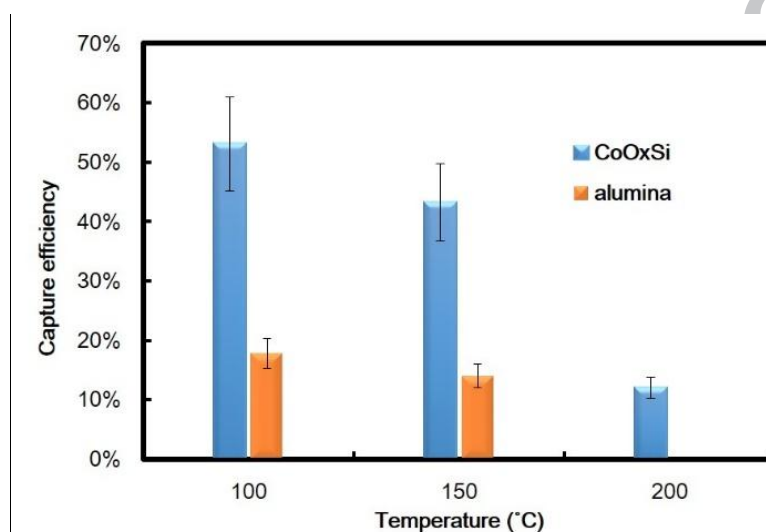


Fig. 5 The comparison of Hg vapour capture rate by CoOxSi xerogel and alumina powder.

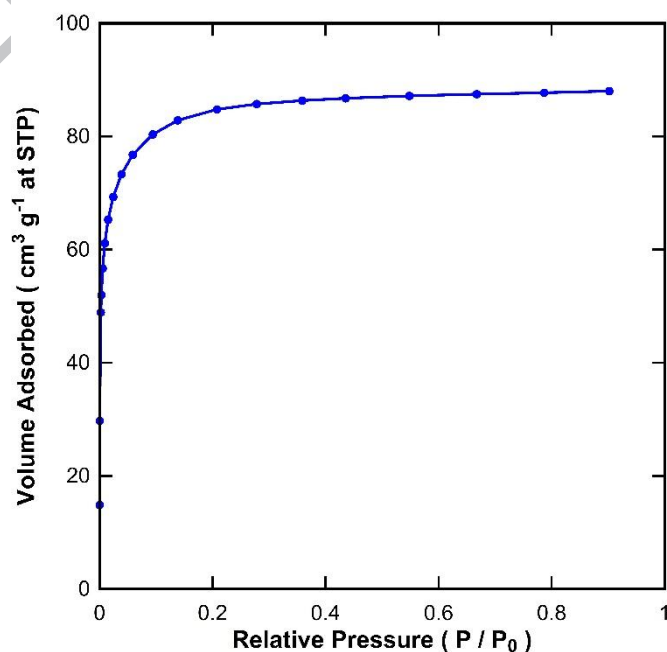


Fig. 6 Nitrogen adsorption (77K) isotherm of CoOxSi xerogel.

The structural property of the CoOxSi xerogels were determined using N<sub>2</sub> adsorption at 77K in a micromeritics TriStar II 3020. The nitrogen isotherm in Fig. 6 exhibits a type I adsorption curve, a characteristic of microporous materials. The micro-pore volume is 0.14 cm<sup>3</sup>g<sup>-1</sup> and BET surface area of CoOxSi is 312.5 m<sup>2</sup>g<sup>-1</sup>, much higher than the surface areas for alumina [32]. The  $\epsilon/k_B$  value of silica (290K) is also larger than that of alumina (108.5 K [33]), which means that silica has a propensity to be more physically adsorptive material than alumina.

In order to understand the effect of Hg adsorption, CoOxSi xerogels were supported on a metal mesh and Hg adsorption was carried out at 100, 200 and 300 °C. For each case, the weight change of each sample was recorded at 5, 10 and 20 minutes. The Hg adsorption results as a function of time are displayed in Fig. 7a. The Hg adsorption quantity decreased with temperature and increased as function of the Hg vapour concentration (Fig. 7b). These two phenomena are in line with most gases and vapour adsorption results. However, the Hg adsorption did not reach equilibrium after 20 minutes, which is longer than most gases. In addition, the testing time was extended to 60 minutes at 300 ng L<sup>-1</sup> at 100°C and the adsorption quantity still increased at the same rate with time as shown in Fig. 7a. Further tests were carried out at lower temperatures, but the quantity of mercury adsorbed reached values in excess of the maximum detection levels and could not be used. The results obtained experimentally strongly suggest that Hg adsorption follows a linear Henry's law relationship (see Fig. 7b), similar to the adsorption of gases on silica xerogels as reported elsewhere [34]. These results suggest that Hg adsorption is in the low coverage region. In addition, in view of the experimental limitations, it is assumed that Hg sorption behaves like gas adsorption on silica materials.

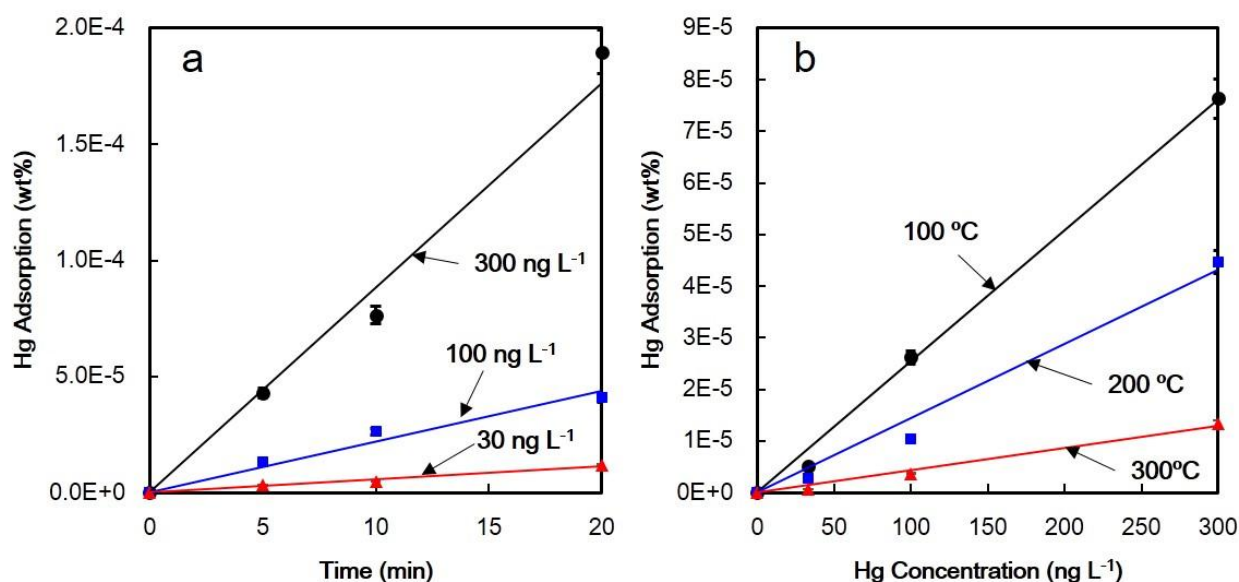


Fig. 7 (a) Hg vapour adsorption ( $\pm 6.95\%$ ) at  $100\text{ }^{\circ}\text{C}$  for different Hg concentration load; (b) Hg vapour adsorption ( $\pm 6.95\%$ ) at the  $10^{\text{th}}$  minute for different temperatures as a function of the Hg concentration.

The LECO analysis was repeated to ensure that all the Hg adsorbed on the samples was accounted for. It was found that the Hg adsorbed on the sample could not be removed completely at a single time analysis and had to be repeated several times. Fig. 8 shows an example where six Hg desorption cycles were necessary. All values in Fig. 7 include the full Hg desorption values. However, it is interesting to note the following desorption trends. The first desorption time generally resulted in 75% desorption of the total Hg adsorbed. This was attributed to Hg adsorbed at the outer surface. The remainder 25% took another five desorption cycles suggesting that Hg diffused very slowly from inner particle to the outer surface. Therefore, these results confirm the low Hg diffusivity in CoOxSi matrices.

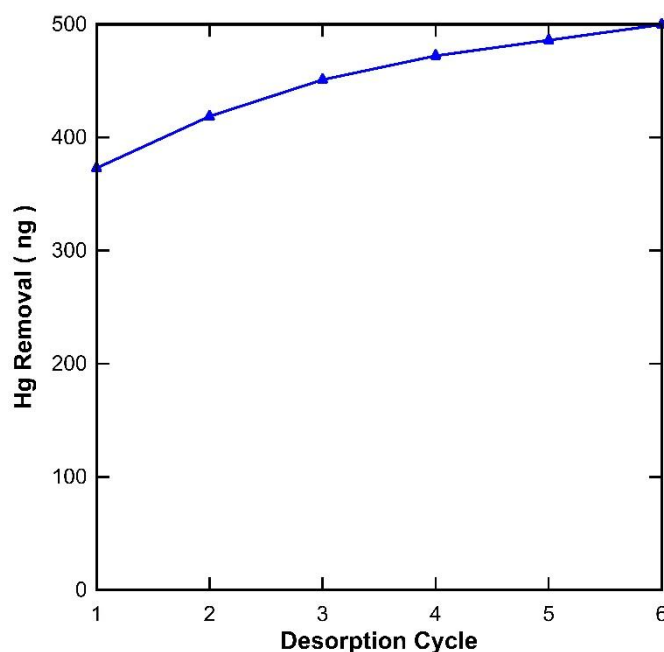


Fig. 8 LECO analysis of sample which was exposed to  $300 \text{ ngHg L}^{-1}$  for 60 min at  $100^\circ\text{C}$ .

The equilibration time for adsorption and/or desorption processes is generally very short (in the order of several  $\mu\text{s}$ ) [35, 36]. Results in Fig. 7a suggest a slow adsorption profile very likely limited by the low diffusivity of Hg in CoOxSi. In this case, there is a common trade-off between adsorbability and mobility for most gases. If a gas easily adsorb on a material, it moves very slowly accordingly. Previous adsorption results and modelling results in Fig. 3 show that Hg has strong affinity to CoOxSi, so the mobility of Hg in CoOxSi is possibly very low. The diffusion of Hg in the micropores is the rate controlling process of this adsorption experiment. Therefore, it is important to develop a model to predict the transient profile adsorption of Hg on CoOxSi matrices. By assuming the powder particle as sphere, the Hg adsorbed concentration profile follows:

$$\frac{\partial q}{\partial t} = \frac{D}{r^2} \frac{\partial}{\partial r} \left( r^2 \frac{\partial q}{\partial r} \right) \quad (17)$$

with boundary condition of  $q=(Kp_{\text{Hg}})/(R_gT)$  at  $r=R_p$  ( $R_p$  is the particle radius). The mean equilibrium constant  $K$  can be estimated from the integration over the volume pore size distribution [37]:

$$K_m = \frac{\int_0^\infty f_v(r_p) \frac{2}{r_p^2} \int_0^{r_p} r \exp\left(-\frac{\phi}{RT}\right) dr dr_p}{\int_0^\infty f_v(r_p) dr_p} \quad (18)$$

The total adsorbed Hg weight to sample weight is:

$$\frac{W_{\text{Hg}}(t)}{W_{\text{sample}}} = \frac{M_{\text{Hg}} \varepsilon_p \int_0^{R_p} 4\pi q(r,t) r^2 dr}{\frac{4\pi}{3} R_p^3 \rho_{\text{sample}}} \quad (19)$$

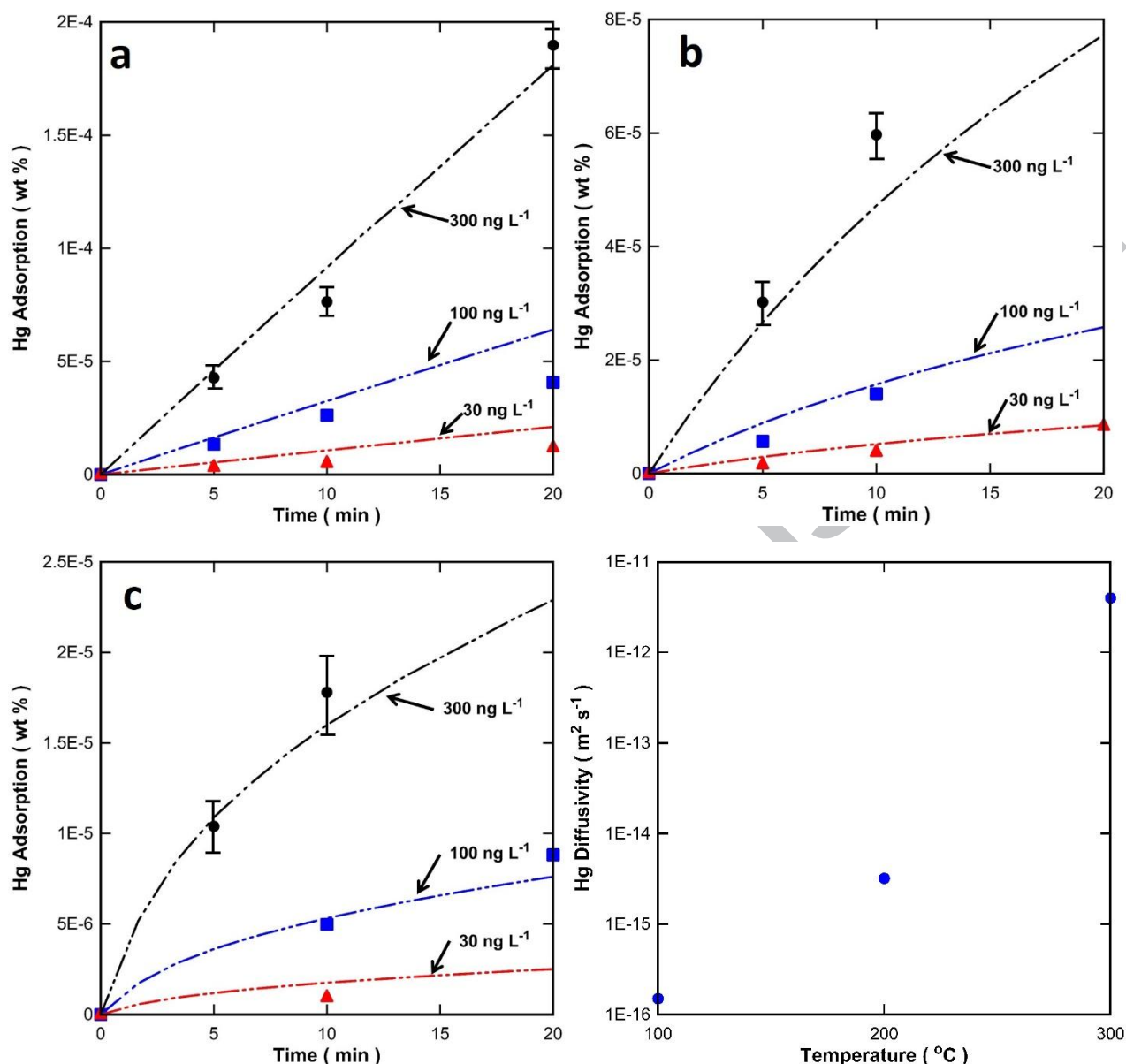


Fig. 9 The adsorption amount ( $\pm 6.95\%$ ) of Hg vapour versus time for different conditions (a) 100°C, (b) 200°C, (c) 300°C, and (d) the fitting diffusivity value

Eq. 19 was used to fit the experimental Hg adsorption values, and the fitting results are shown in Figs. 9a to c. The modelling results fitted quite well the experimental results, where under or over prediction is minimal. Fig. 9d shows the diffusivity value obtained by Eq. (19) from fitting the experimental data. The Hg diffusivity is very low and the adsorbed Hg on the surface needs a long time to diffuse to the inside of the sample particle. The Hg diffusivity fitting result is also supported by the slow desorption evidenced by the experimental results in Fig. 8.

#### 4.2 Permeation test of CoOxSi membrane

The permeation of both pure N<sub>2</sub> and N<sub>2</sub>+Hg vapour mixture through a CoOxSi membrane was measured at feed pressures  $\sim 2.7$  bar, whilst the permeate side was kept at 1 bar. The temperature

was varied from 100 to 300°C. Fig. 10 shows that the permeance of pure N<sub>2</sub> decreased as a function of temperature for a CoOxSi membrane. This is a common trend for the permeance of pure N<sub>2</sub> in high quality ultra-microporous silica derived membranes [22]. This is generally associated with a negative apparent activation energy, equivalent to -15.9 kJ mol<sup>-1</sup> for the results shown in Fig. 10. Contrary to this trend, the addition of Hg to the N<sub>2</sub> gas stream resulted in significant changes, as the permeation of N<sub>2</sub> became almost constant with increasing temperature. Hence, the apparent activation energy increased to values close to 0.0 kJ mol<sup>-1</sup>.

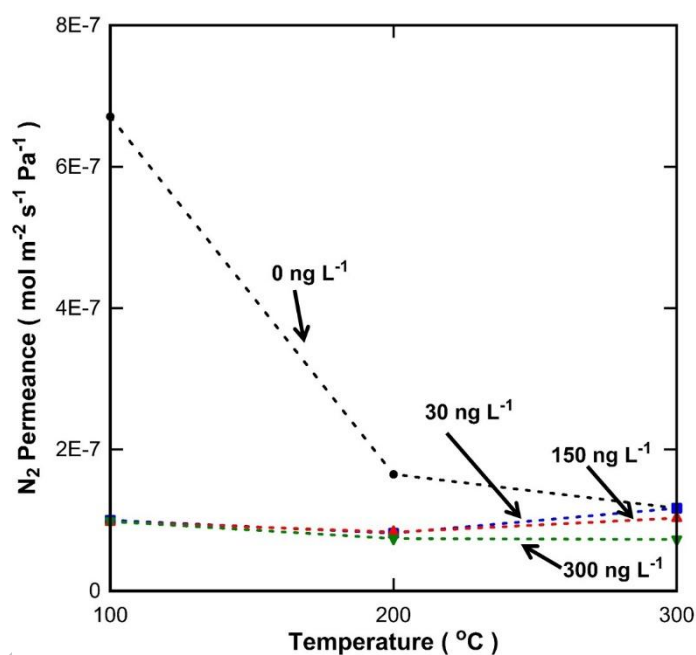


Fig. 10. The permeance ( $\pm 2\%$ ) of N<sub>2</sub> for various feed gas Hg concentration and temperatures.

Table 2 lists the average flow rates of Hg through the membrane. It is interesting to note that the Hg flow rate increase is almost proportional to the Hg concentration load. For instance, the Hg flow rates increase an average 5.06 times (30 to 150 ng L<sup>-1</sup>), and 9.1 (30 to 300 ng L<sup>-1</sup>). Although measuring Hg flow rates at ng s<sup>-1</sup> is susceptible to experimental variation, which tends to decrease with increasing Hg concentration as given in Table 2. This experimental variation is significant compared with that for gas permeation which has simpler measurement steps and is much easier to control. In the case of Hg permeation, apart from the conventional permeation variation of  $\pm 10\%$ , this value is compounded by variations in the Hg emission source, sample weight measurement and the Hg spectrometry variations.

Table 2 – Average Hg flow rates for CoOxSi membrane as a function of various Hg loading.

Hg concentration (ng L <sup>-1</sup> )	30	150	300
Hg average flow rate (ng s <sup>-1</sup> )	7.6×10 <sup>-4</sup>	3.9×10 <sup>-3</sup>	7.0×10 <sup>-3</sup>
Experimental variation	75%	50%	14%

#### 4.2 Oscillator + EMT model validation

The oscillator model results in Fig. 11a indicate that N<sub>2</sub> permeability is a decreasing function with respect to temperature when the silica pores are larger than 0.32nm. When the pore size is smaller than 0.32nm, the permeability of N<sub>2</sub> should increase with temperature. Since the permeability is defined as  $\frac{DK}{R_g T}$  in this model, the permeability variation with temperature is explained by separating  $D$  and  $\frac{K}{R_g T}$  terms as depicted in Fig. 11b. The diffusion coefficient is a monotonically increasing function with respect to temperature and also to pore size which can be evaluated by Eqs. (1) and (5).

However, the Henry's constant  $\frac{K}{R_g T}$  in Fig. 11 shows a more complicated trend, which generally increases as a function of pore size in the considered range but does not follow a single trend as a function of temperature. It should be noted that  $\frac{K}{R_g T}$  increases with temperature when pore sizes are < 0.32nm, and decreases with temperature for pore sizes > 0.32nm. Due to adsorption principles, the gas concentration in nano-pores generally decreases with temperature, so  $\frac{K}{R_g T}$  should be a decreasing function of temperature. However, the results show an opposite trend for the pores < 0.32nm. This is attributed to the high potential in the smaller pores, as the gas molecules need high kinetic energy to squeeze into these tiny pores. As the kinetic energy increases with temperature, so does the gas concentration for pores < 0.32nm. The effect of temperature and pore size is significantly higher on  $\frac{K}{R_g T}$  than that on  $D$ , so the permeability  $\frac{DK}{R_g T}$  as a function of temperature is dominated by  $\frac{K}{R_g T}$ . In other words, the point of intersection of different temperatures was found at pore sizes equal to 0.32 nm, and permeability will increase with temperature at smaller pore sizes, contrary to the decrease in permeability for the larger pore sizes.

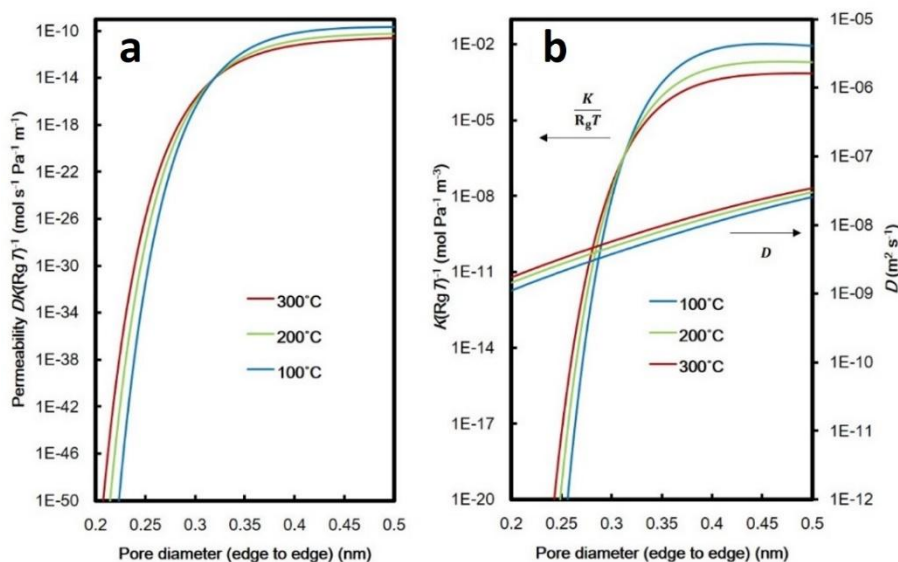


Fig. 11 (a) N<sub>2</sub> permeability  $\frac{DK}{R_g T}$  to pore size predicted by Oscillator model; (b) Diffusion

coefficient  $D$  and Henry's constant  $\frac{K}{R_g T}$  to pore size modelled by Oscillator

The PSD in Fig. 2 suggested that pores of the silica membrane consist of both pores  $> 0.32$ nm and pores  $< 0.32$ nm. However, pure N<sub>2</sub> permeation showed a decreasing with temperature in Fig. 10, implying that the total permeate flow is dominated by the permeation through pores with diameters larger than 0.32 nm. This is because the flow contribution from each pore size is not proportional to the number of pores. Larger pores have a higher contribution to the total permeation flow, accounting for a higher portion in the total permeability. For example the permeance of a 0.35 nm single pore is 2531 times higher than that of a 0.31 nm single pore based on the oscillator prediction.

The changes in transport phenomena observed experimentally in Fig. 10 strongly suggest that Hg affects the diffusion or adsorption of N<sub>2</sub>. Therefore, the Oscillator+EMT models discussed above were used to explain the interesting Hg effect of N<sub>2</sub> permeation phenomenon changes. Since the information of membrane thickness  $L$ , membrane porosity  $\varepsilon_p$  and pore tortuosity  $\tau_t$  in Eq. (9) are difficult to obtain, a dimensionless flux  $J_{DML}$  is used instead of absolute permeation flux:

$$J_{DML} = \frac{J}{J_{T=100^\circ\text{C}, H_g=0}} \quad (20)$$

where  $J_{DML}$  is a dimensionless flux,  $J$  is the N<sub>2</sub> gas flux and  $J_{T=100^\circ\text{C}, H_g=0}$  is the pure N<sub>2</sub> gas flux at 100 °C without any Hg loading. The dimensionless flux using Eq. (20) and the experimental gas permeation results in Fig. 10 are compared in Fig. 12. The Oscillator+EMT model gives reasonable

fitting to the experimental observation. It is interesting to observe that the presence of Hg vapour reduced the permeance of N<sub>2</sub> by 85.4% at 100 °C and 55.0% at 200 °C. However, this effect is not significant at 300 °C.

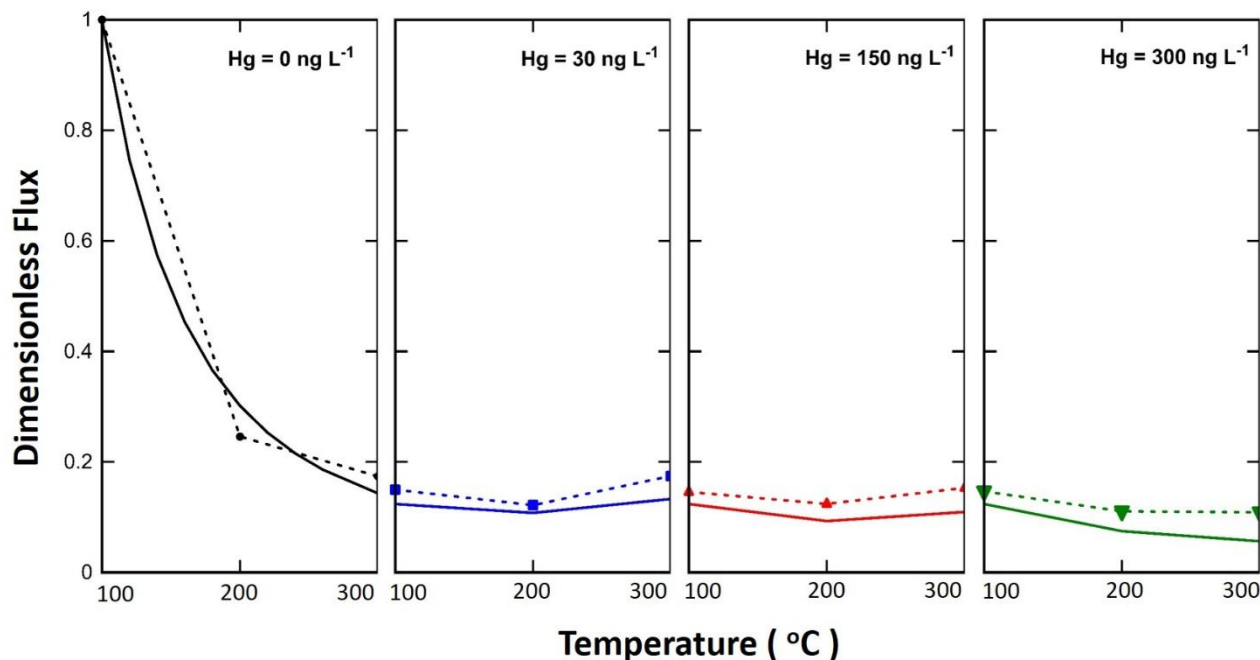


Fig. 12 The dimensionless flux of pure N<sub>2</sub>+Hg vapours at various temperatures and Hg loading: experimental results (symbol plus broken line) and Oscillator EMT simulation (full line).

The results in Fig. 12 together with Fig. 4 strongly suggest that the effective pore size distribution for N<sub>2</sub> permeation at different temperatures has changed by Hg adsorption. This can only be attributed to Hg adsorption, thus reducing the pore size for N<sub>2</sub> permeation. As shown in Fig. 7 and Fig. 9, Hg adsorbed more strongly at lower temperatures than at higher temperatures. The Hg adsorption results therefore correlate well with the reduction of N<sub>2</sub> permeation at 100 and 200 °C, whilst the low Hg adsorption at 300 °C did not affect N<sub>2</sub> permeation.

The effect of Hg sorption on N<sub>2</sub> permeation can be further explained by considering the effect of temperature. The Hg sorption at 100 °C was stronger and significantly contributed to pore blockage or the reduction of the average pore sizes. Hence, the N<sub>2</sub> permeance significantly reduced from pure N<sub>2</sub> to N<sub>2</sub>+Hg vapour permeation. However, Hg adsorption was very weak at 300 °C, and the effect of Hg blocking pores or reducing the average pore sizes was negligible.

A further consideration is on the Hg concentration changes from 30 to 300 ng L<sup>-1</sup> in the total performance of the membrane. Fig. 7b shows that the adsorbed Hg concentration is approximately

proportional to the feed Hg vapour concentration. These results would suggest that the number pores blocked or the reduction of average pore sizes would increase as a function of the Hg concentration load in the N<sub>2</sub>+Hg mixture. However, Table 1 showed that Hg flow rates increase an average 5.06 times (30 to 150 ng L<sup>-1</sup>), and 9.1 (30 to 300 ng L<sup>-1</sup>). These results indicate that Hg is not continuously accumulating in the membrane, and tends to follow adsorption and desorption equilibrium, similar to the Henry's law adsorption.

Nevertheless, the N<sub>2</sub> permeation did not reduce with increasing the Hg concentration load in the gas mixture. In principle, it would be logical to assume that as the Hg concentration increases, it will likely reflect the blockage of more pores. However, this is not the case. The first reason is that Hg is strongly attracted to another Hg molecule. So if a small pore (2.5-4.0Å) is already blocked by a Hg molecule, there is a high probability of another new Hg molecule entering the same pore. This means the likelihood of a new Hg molecule going to another empty pore is relatively low compared to joining a pore already occupied by Hg. In addition, for the large pores (6.7-7.8Å and 12-14Å), there is high probability that Hg will be coalescing with the Hg molecules already adsorbed on these pores. As the N<sub>2</sub> permeance does not decrease with the increase in Hg loading (and likewise Hg adsorption), these results strongly suggest that the coalescence of Hg molecules occurs along the pore wall rather than radially. Hg coalescence radially would cause more pore blockage and major reduction in N<sub>2</sub> flux which is not the case as proved by the experimental results described.

Finally, this model could be applied for other gases such as H<sub>2</sub>. The permeation of gases across silica membrane mainly depends on the physical property of gases, especially the Lennard-Jones diameter ( $\sigma$ ). The Lennard-Jones diameter of H<sub>2</sub> is smaller than N<sub>2</sub>, and the consequence of this difference is that H<sub>2</sub> always shows higher permeation than N<sub>2</sub>. Nevertheless, if the pore is blocked by Hg adsorption, H<sub>2</sub> cannot permeate either even if H<sub>2</sub> is more permeable. Therefore, the permeation of H<sub>2</sub> and any other gas are likely to be reduced due to Hg pore blockage, though the H<sub>2</sub> permeation will be always higher than N<sub>2</sub> permeation tested under similar conditions and using high quality silica membranes delivering high H<sub>2</sub>/N<sub>2</sub> selectivity.

## 5. Conclusion

This work shows for the first time that the N<sub>2</sub> permeation in microporous silica derived membranes was significantly affected by the presence of Hg vapour. This was attributed to the strong Hg adsorption even though Hg concentration loading was varied from extremely low 30 to a maximum 300 ng L<sup>-1</sup>. The presence of Hg greatly reduced N<sub>2</sub> permeance by 85.4% at 100°C and 55.0% at 200

°C. However, this effect was not significant at 300°C due to weak Hg adsorption. Hence, there was a correlation between increased Hg adsorption and decreased N<sub>2</sub> permeance. The oscillator model together with the effective medium theory (EMT) were applied to understand the unusual N<sub>2</sub> transport phenomena changes. The pure N<sub>2</sub> permeate flux across the CoOxSi membrane decreased as a function of temperature, indicating a negative apparent activation energy. The oscillator model suggests that pure N<sub>2</sub> permeation is dominated by pores larger than 0.32nm due to the negative apparent activation energy for N<sub>2</sub> permeation. The observed reduction in N<sub>2</sub> permeation with Hg exposure suggests that Hg adsorption blocked pores (2.5-4.0Å) or narrowed the size of larger pores (6.7-7.8Å and 12-14Å).

In principle, Hg tends to seek the lower potential which is associated with the diffusion into pores ~0.38nm. In view of the amorphous nature of silica matrices, gas permeation is also thermodynamically favoured into low energy levels, meaning at larger pores. Hence, very likely Hg adsorption occurred at large pores, thus reducing the average pore sizes for N<sub>2</sub> permeation. In addition, increasing the feed Hg concentration from 30 to 300ng L<sup>-1</sup> in the gas mixture did not decrease the N<sub>2</sub> permeation. It was found that Hg did not accumulate in the membrane matrix, as average Hg flow rates increased at the same ratios as the Hg concentration loading in the feed gas mixture. Hence, the increase in Hg adsorption coverage was attributed to preferential Hg molecule adsorption in small pores (2.5-4.0Å) or clustering along the pore wall for large pores (6.7-7.8Å and 12-14Å).

#### Nomenclature

$c$	gas concentration (mol m <sup>-3</sup> )
$D$	diffusivity (m <sup>2</sup> s <sup>-1</sup> )
$F$	flowrate (mol s <sup>-1</sup> )
$f_N$	number density distribution (nm <sup>-1</sup> )
$f_v$	volume density distribution (nm <sup>-1</sup> )
$g_N$	number density distribution after some pore is blocked by Hg (nm <sup>-1</sup> )
$K$	equilibrium constant
$K_m$	mean equilibrium constant
$k_B$	Boltzmann constant (J K <sup>-1</sup> )
$L$	membrane thickness (nm)
$l$	pore length (nm)
$M$	molar mass (kg mol <sup>-1</sup> )

$m$	molecular weight (kg)
$N$	number of molecules in a pore
$N_A$	Avogadro's constant ( $6.022 \times 10^{23} \text{ mol}^{-1}$ )
$P$	probability of a pore not being blocked by Hg
$p$	pressure (Pa)
$p_r$	radial momentum ( $\text{kg m s}^{-1}$ )
$p_z$	axial momentum ( $\text{kg m s}^{-1}$ )
$p_\theta$	tangential momentum ( $\text{kg m s}^{-1}$ )
$q$	concentration inside pore ( $\text{mol m}^{-3}$ )
$R_g$	gas constant ( $\text{J mol}^{-1} \text{ K}^{-1}$ )
$R_p$	particle radius (m)
$r$	radial coordinate (m)
$r_{c1}$	radial coordinate where hopping commences (m)
$r_{co}$	radial coordinate where radial momentum is zero (m)
$r_p$	pore size (m)
$S$	perm-selectivity
$T$	temperature (K)
$t$	time (s)
$W$	weight (kg)
Greek letters	
$\varepsilon$	Lennard Jones well depth (J)
$\varepsilon_p$	membrane porosity
$\eta$	areal density of sites on the pore surface ( $\text{m}^{-2}$ )
$\theta$	angular coordinate
$\lambda$	mass transfer conductance ( $\text{mol s}^{-1} \text{ Pa}^{-1}$ )
$\mu$	chemical potential ( $\text{J mol}^{-1}$ )
$\rho_{\text{sample}}$	sample density ( $\text{kg m}^{-3}$ )
$\sigma$	Lennard Jones collision diameter (nm)
$\tau$	hopping time (s)
$\tau_t$	tortuosity
$\phi$	potential (J)

## Acknowledgement

The authors acknowledge financial support from the Centre for Low Emission Technology, the Queensland Government via the NIRAP funding scheme, and the Australian Research Council (DP110101185). The authors thank Dr. Simon Smart and Dr. Christelle Yacou from the School of Chemical Engineering, The University of Queensland, for preparing the cobalt oxide silica xerogels and membranes tested in this work. J. C. Diniz da Costa gratefully thanks the support given by the ARC Future Fellowship Program (FT130100405).

## Reference

- [1] R.M. de Vos, H. Verweij, Improved performance of silica membranes for gas separation, *J. Membr. Sci.* 143 (1998) 37-51.
- [2] A.J. Burggraaf, Single gas permeation of thin zeolite (MFI) membranes: theory and analysis of experimental observations, *J. Membr. Sci.* 155 (1999) 45-65.
- [3] R.M. Barrer, Porous Crystal Membranes, *J. Chem. Soc. Faraday Trans.*, 86 (1990) 1123-1130.
- [4] V.P. Zhdanov, General equations for description of surface diffusion in the framework of the lattice-gas model, *Surface Science Letters*, 149 (1985) L13-L17.
- [5] J. Xiao, J. Wei, Diffusion mechanism of hydrocarbons in zeolites—I. Theory, *Chem. Eng. Sci.* 47 (1992) 1123-1141.
- [6] J. Xiao, J. Wei, Diffusion mechanism of hydrocarbons in zeolites—II. Analysis of experimental observations, *Chem. Eng. Sci.* 47 (1992) 1143-1159.
- [7] A. Darmawan, J. Motuzas, S. Smart, A. Julbe, J.C. Diniz da Costa, Binary iron cobalt oxide silica membrane for gas separation, *J. Membr. Sci.* 474(2015) 32–38.
- [8] S. Gopalakrishnan, Y. Yoshino, M. Nomura, B.N. Nair, S.-I. Nakao, A hybrid processing method for high performance hydrogen-selective silica membranes, *J. Membr. Sci.* 297 (2007) 5-9.
- [9] T. Yoshioka, E. Nakanishi, T. Tsuru, M. Asaeda, Experimental studies of gas permeation through microporous silica membranes, *AIChE J.* 47 (2001) 2052-2063.
- [10] R. Krishna, J.M. van Baten, Influence of adsorption on the diffusion selectivity for mixture permeation across mesoporous membranes, *J. Membr. Sci.* 369 (2011) 545-549.
- [11] R.S.A. Lange de, K. Keizer, A.J. Burggraaf, Analysis and theory of gas transport in microporous sol-gel derived ceramic membranes, *J. Membr. Sci.* 104 (1995) 81-100.
- [12] R. Igi, T. Yoshioka, Y.H. Ikuhara, Y. Iwamoto, T. Tsuru, Characterization of Co doped silica for improved hydrothermal stability and application to hydrogen separation membranes at high temperatures, *J. Am. Ceram. Soc.* 91 (2008) 2975-2981.

- [13] L. Liu, D.K. Wang, D.L. Martens, S. Smart, J.C. Diniz da Costa, Interlayer-free microporous cobalt oxide silica membranes via silica seeding sol-gel technique, *J. Membr. Sci.* 492 (2015) 1–8.
- [14] V. Boffa, J.E. ten Elshof, A.V. Petukhov, D.H.A. Blank, Microporous Niobia–Silica Membrane with Very Low CO<sub>2</sub> Permeability, *ChemSusChem* 1 (2008) 437-443.
- [15] B. Deonarine, G. Ji, S. Smart, J.C. Diniz da Costa, G. Reed, M. Millan, Ultra-microporous membrane separation using toluene to simulate tar-containing gases, *Fuel Proc. Technol.* 161 (2017) 259-264.
- [16] T. Yoshioka, T. Tsuru, M. Asaeda, Condensable vapor permeation through microporous silica membranes studied with molecular dynamics simulation, *Sep. Purif. Technol.* 32 (2003) 231-237.
- [17] A.J. Huth, J.M. Stueve, V.V. Gulians, A simulation study of the gas separation properties of decadodecasil 3R zeolite with emphasis on energy-related separations, *J. Membr. Sci.* 403–404 (2012) 236-249.
- [18] S. Smart, C.X.C. Lin, L. Ding, K. Thambimuthu, J.C. Diniz da Costa, Ceramic membranes for gas processing in coal gasification, *Energy Environ. Sci.* 3 (2010) 268-278.
- [19] J.H. Pavlish, Status review of mercury control options for coal-fired power plants, *Fuel Proc. Technol.* 82 (2003).
- [20] F. Frandsen, K. Dam-Johansen, P. Rasmussen, Trace elements from combustion and gasification of coal—An equilibrium approach, *Prog. Energy Combust. Sci.* 20 (1994) 115-138.
- [21] R. Krishna, R. Baur, Analytic solution of the Maxwell-Stefan equations for multicomponent permeation across a zeolite membrane, *Chem. Eng. J.*, 97 (2004) 37-45.
- [22] C. Yacou, S. Smart, J.C. Diniz da Costa, Long term performance cobalt oxide silica membrane module for high temperature H<sub>2</sub> separation, *Energy Environ. Sci.*, 5 (2012) 5820-5832.
- [23] M.C. Duke, S.J. Pas, A.J. Hill, Y.S. Lin, J.C. Diniz da Costa, Exposing the molecular sieving architecture of amorphous silica using positron annihilation spectroscopy, *Adv. Funct. Mater.* 18 (2008) 3818-3826.
- [24] T. Yoshioka, A. Yasumoto, K. Kishi, T. Tsuru, MD simulation studies for effect of membrane structures and dynamics on gas permeation properties through microporous amorphous silica membranes, *Desalination* 233 (2008) 333-341.
- [25] T. Yoshioka, T. Tsuru, M. Asaeda, Molecular dynamics study of gas permeation through amorphous silica network and inter-particle pores on microporous silica membranes, *Mol. Phys.* 102 (2004) 191-202.

- [26] P. Hacıoğlu, D. Lee, G.V. Gibbs, S.T. Oyama, Activation energies for permeation of He and H<sub>2</sub> through silica membranes: An ab initio calculation study, *J. Membr. Sci.* 313 (2008) 277-283.
- [27] G.J. Tjatjopoulos, D.L. Feke, J.A. Mann, Molecule-micropore interaction potentials, *J. Phys. Chem.* 92 (1988) 4006-4007.
- [28] A.B. Shelekhin, A.G. Dixon, Y.H. Ma, Theory of gas diffusion and permeation in inorganic molecular-sieve membranes, *AIChE J.*, 41 (1995) 58-67.
- [29] G. Raabe, R.J. Sadus, Molecular simulation of the vapor-liquid coexistence of mercury, in.
- [30] S.K. Bhatia, Modeling Pure Gas Permeation in Nanoporous Materials and Membranes, *Langmuir* 26 (2010) 8373-8385.
- [31] B. Stefanov, O. Jordanov, L. Zarkova, Interaction potential in  $1 \Sigma_g + Hg 2$  : fit to the experimental data, *J. Phys. B: Atomic Mol. Phys.* 15 (1982) 239.
- [32] X. Gao, M.R. Bonilla, J.C. Diniz da Costa, S.K. Bhatia, The transport of gases in a mesoporous  $\gamma$ -alumina supported membrane, *J. Membr. Sci.* 428 (2013) 357-370.
- [33] F.J. Blas, Modeling new adsorbents for ethylene/ethane separations by adsorption via  $\pi$ -complexation, *Fluid Phase Equilib.* 150-151 (1998).
- [34] H.H. El-Feky, K. Briceño, E.d.O. Jardim, J. Silvestre-Albero, T. Gumí, Novel silica membrane material for molecular sieve applications, *Microporous Mesoporous Mater.* 179 (2013) 22-29.
- [35] B.K. Sadik Kakaç, F.A. Kulacki, F. Arinç, Convective Heat and Mass Transfer in Porous Media, in: NATO ASI Series, Springer Netherlands, 1991.
- [36] A.G. Fedorov, R. Viskanta, Analysis of transient heat/mass transfer and adsorption/desorption interactions, *Int. J. Heat Mass Transfer* 42 (1999) 803-819.
- [37] X. Gao, J.C. Diniz da Costa, S.K. Bhatia, Understanding the diffusional tortuosity of porous materials: An effective medium theory perspective, *Chem. Eng. Sci.* 110 (2014) 55-71.

## Investigation and Simulation of the Transport of Gas Containing Mercury in Microporous Silica Membranes

Guozhao Ji<sup>a,b</sup>, Anthe George<sup>c,d</sup>, Vicky Skoulou<sup>c,e</sup>, Graham Reed<sup>c</sup>, Marcos Millan Agorio<sup>c</sup>, Kamel Hooman<sup>f</sup>, Suresh K. Bhatia<sup>a</sup>, João C. Diniz da Costa<sup>a\*</sup>

### Highlights

- Condensable Hg vapour effect on N<sub>2</sub> permeation in microporous silica membrane.
- Significant Hg effect at 100 and 200 °C, though negligible at 300 °C.
- Hg effect correlated well with Hg adsorption on microporous silica xerogels.
- Oscillator model for gas transport including the Effective Medium Theory (EMT).
- The model's simulated results fitted well experimental results.

## Investigation and Simulation of the Transport of Gas Containing Mercury in Microporous Silica Membranes

Guozhao Ji<sup>a,b</sup>, Anthe George<sup>c,d</sup>, Vicky Skoulou<sup>c,e</sup>, Graham Reed<sup>c</sup>, Marcos Millan Agorio<sup>c</sup>, Kamel Hooman<sup>f</sup>, Suresh K. Bhatia<sup>a</sup>, João C. Diniz da Costa<sup>a\*</sup>

### Graphical Abstract

